Contents lists available at ScienceDirect

Journal of Solid State Chemistry

journal homepage: www.elsevier.com/locate/jssc

A new 3D Ho^{III}-organic framework constructed from 1,3,5-tris(4-carboxyphenyl)benzene and 1,10-phenanthroline: Crystal structure, morphological and solid state luminescence properties

Mustafa Burak Coban

Center of Sci. and Tech. App. and Research, Balikesir University, 10145, Balikesir, Turkey

A B S T R A C T

A new polynuclear Ln^{III} coordination compound (**1**) with the stoichiometric formula $\{[Ho(BTB)(phen)]\cdot(DMF)\}_n$, (H$_3$BTB = 1,3,5-Tris(4-carboxyphenyl)benzene, phen = 1,10 –phenanthroline monohydrate and DMF = N, N – dimethylformamide) has been synthesized by the solvothermal method and characterized by the infrared spectroscopy, thermogravimetric analysis, single-crystal X-ray diffraction studies, elemental analysis and solid-state electronic absorption properties and solid-state photoluminescence measurements. The XRD analyses indicate that **1** crystallizes in a monoclinic system with space group P2$_1$/c and also each Ho^{III} ion has eight coordination, forming a distorted square antiprismatic geometry. For all the coordinated oxygen atoms, six of them belong to five carboxylate groups from different BTB^{3-}ligands, while two nitrogen atoms from only one phen ligand were involved in the coordination. Two crystallographically equivalent Ho^{III} ions are bridged to a dimeric unit as secondary unit buildings (SUBs) by four carboxyl groups in different directions, which also form typical 1D hexagonal channels with BTB^{3-} ligands, these channels are connected in a three-dimensional (3D) framework. Also, these open channels were occupied by two different BTB^{3-} ligands. According to the 3D Hirshfeld surface and 2D fingerprint plots analysis, H···H intermolecular interactions are the dominant interactions in the Ho^{III}. Additionally, the π···π stacking information determined by the shape index and curvedness plots coincides with the crystal structure analysis. Moreover, photoluminescence properties of **1** were recorded and investigated at room temperature in the Vis-NIR region. Under the excitation of UV light, **1** exhibited strong yellowish-orange emission with CIE chromaticity coordinates (0.480, 0.430). **1** emits at 521, 575 and 653 nm correspond to $^5F_3 \rightarrow {}^5I_8$, $^5S_2 + {}^5F_4 \rightarrow {}^5I_8$ and $^5F_5 \rightarrow {}^5I_8$ in the visible region, whereas only one weakly peak at 761 nm originated to $^5S_2 + {}^5F_4 \rightarrow {}^5I_7$ in the NIR region. This polymeric complex can potentially be applied to luminescent probes or OLEDs.

1. Introduction

Over the past decade, lanthanide-based compounds or lanthanide-organic frameworks (LOFs) have attracted growing attention due to their aesthetically and intriguing properties [1] and also their several potential applications such as luminescent probes in biomedical [2,3], gas storage and separation [4], sensors [5], drug delivery [6], upconversion materials [7,8], lasers, heterogeneous catalysis [9,10] and solar energy conversion [11]. Besides, trivalent lanthanide organic frameworks have been studied in depth because of the special optical and magnetic properties of Ln^{III} ions, which come from their unique 4f electronic configurations [12]. Lanthanide-based polymers are being investigated as molecular magnetic materials, as many lanthanide ions have unquenched orbital angular momentum that causes magnetic

anisotropy and has a large number of unpaired 4f electrons resulting in high spin [13]. Lanthanide organic frameworks emit luminescence at different wavelengths in the electromagnetic spectrum, which plays a crucial role in solid-state lighting and imaging fields [14–17]. As a result, they exhibit abundant emission colors attributed to 4f–4f or 5d–4f transitions [18,19]. Moreover, Ln-MOFs can exhibit not only strong characteristic luminescence emissions of lanthanide ions, but also photoluminescence properties due to the "antenna effect" of spacer ligands [20].

The solvothermal reaction is one of the most well-known useful techniques for the construction of crystalline metal-organic frameworks. This system can greatly increase the dissolution distribution and chemical reaction activity of the reactants, which can ensure the reaction takes place at lower temperatures. Another advantage of the solvothermal

process is the product prepared by this way higher purity and uniformity [21,22].

A successful synthetic approach to isolate discrete 4f-metal-ion complexes such as polynuclear entities is the simultaneous use of mono- and/or bidentate bridged anionic species and chelating organic ligands. For the anionic groups, carboxylate ligands are commonly chosen because of the interaction of carboxylate groups with Ln^{III} ions [23–27]. Another effective approach, for the synthetic advantage of metal-organic frameworks, is to incorporate a second organic ligand such as 1,10-phenanthroline, 4,4′-bipyridine, or 2,2′-bipyridine into the structures [28–33].

The high coordination number of lanthanide ions could benefit the formation of nodes with multiple connections and solvent occupied potential open metal sites, which could result in high dimensional framework structure with unique topology, versatile architecture and crystal packing motifs. Besides that, the characteristic fluorescence emissions of lanthanide ions, which are readily detectable and distinguishable for their high intensity and specific emission wavelength, are ideal candidate for sensing applications. Ho^{III} compound, the free ligands act as a strong sensitizer, efficiently transferring the excitation energy from ligands to the Ho^{III} ions, thus making this compound splendid candidate for efficient luminescent materials without the quenching effects of solvent molecules. In this sense, **1** will be able to offer a wide range of uses in technological applications by giving luminescence signals in a wide spectral region. Keeping in mind above mentioned ideas and also as part of ongoing research, our group was motivated to identify new lanthanide compounds designed with efficient antenna ligands to probe the sensitized both visible and NIR luminescence. Herein, in the context of our systematic studies on polydentate antenna ligands containing lanthanide compounds, the aiming at checking the ability of rare-earth ions to afford high-dimensional materials and to investigate photoluminescence behaviour in the wide spectral region.

To the best of our knowledge, only three Ln-MOFs associated with the H$_3$BTB and phen ligand were investigated [34–36]. It was observed that gas adsorption was mainly studied. However, there are no systematic reports on the crystal structure and photoluminescence properties of the Ho^{III} complex coordinated H$_3$BTB and phen ligands.

Here, {[Ho(BTB)(phen)]·(DMF)}$_n$ containing the ligands 1,3,5-Tris(4-carboxyphenyl) benzene (H$_3$BTB) and 1,10-phenanthroline monohydrate (phen) was solvothermally synthesized and crystal structure, thermogravimetric analysis, solid-state absorption and luminescence properties, infrared spectroscopy, Hirshfeld surface and morphology properties of the compound were reported.

2. Experimental section

2.1. Materials and measurements

The analytic-grade starting reagents: Holmium(III) chloride hexahydrate (HoCl$_3$·6(H$_2$O), Sigma&Aldrich; ≥99.0% pure), H$_3$BTB (1,3,5-Tris(4-carboxyphenyl)benzene, Sigma&Aldrich; ≥98.0% pure), phen (1,10-phenanthroline monohydrateSigma&Aldrich; 99.0% pure) and DMF (N,N–Dimethylformamide Sigma&Aldrich; 99.8% pure). Fourier transform infrared spectroscopy (FT-IR) were performed on a PerkinElmer Spectrum 65 spectrophotometer in the wavenumber range 4000–600 cm^{-1} at room temperature. The electronic absorption spectra of solid powder samples were measured by an Ocean Optics Maya 2000Pro Spectrometer range from 200 to 575 nm at room temperature. Thermal stability was studied on a PerkinElmer TGA 4000 thermogravimetric analyzer with a heating rate of 10 °C min^{-1}, under a controlled nitrogen atmosphere and a temperature range from ambient to 800 °C. Elemental analysis for (C, H and N) was executed out on CHNS-932 Leca analyzer. Powder X-ray diffraction of the samples was obtained by a Philips PW-1710/00 diffractometer using Cu-K$_\alpha$ radiation (λ = 1.5418 Å). The surface morphology analyses were conducted using Carl Zeiss SUPRA-55 Field Emission Environmental Scanning Electron Microscope

(FESEM) instrument. The PL properties of the host regents and synthesized compound measurements in the broad spectral region. The PL data were obtained using an ANDOR SR500i-BL photoluminescence spectrometer, which is equipped with an air-cooled CCD camera as a detector. Laser excitation emitted by a 5ns frequency Nd:YLF pulsed laser at λ = 349 nm was used. Powder samples were put in a brass sample holder during the PL measurements.

2.2. Solvothermal self-assembly synthesis of **1**

Solvothermal reactions have been a well-known and powerful approach in the synthesis of rare-earth/ligand structures for many years and have also been widely adopted in the preparation of versatile lanthanide organic frameworks that exhibits intriguing structural diversity and promising potential applications in the past years [37]. Further, during a specific solvothermal process, many parameters can affect the crystallization of the final product, such as solvents molecules, pH values, reaction duration, and temperature. Considering the above factors, reaction temperature has a great influence on the yield of **1**.

Single crystals of {[Ho(BTB)(phen)]·(DMF)}$_n$ (**1**) were successfully obtained by a solvothermal method (see Scheme 1). In this synthesis, HoCl$_3$·6(H$_2$O) (0.0379 g, 0.1 mmol), H$_3$BTB (0.0438 g, 0.1 mmol) and phen (0.0594 g, 0.3 mmol) were dissolved in dimethylformamide (DMF, 10 ml) and H$_2$O (5 ml). The solution was vigorously stirred by magnetic stirring for about 2 h and then the reaction mixture was transferred in a 45 ml Teflon-lined stainless steel autoclave. The autoclave was heated at 120 °C for 5 days in an electrical oven. then cooled to room temperature at a rate of 5 °C/h under ambient conditions. After cooling to ambient temperature, the light yellow crystals were collected, washed with DMF several times and dried (72% yields.) Elemental Analysis C$_{42}$H$_{30}$HoN$_3$O$_7$ (%) Calcd for compound **1**: C: 51.64, H: 6.62, N: 10.87. Found: C: 51.59, H: 6.64, N: 10.84.

2.3. Single-crystal X-ray studies

Diffraction measurements were made on an Xcalibur Eos diffractometer equipped with MoKα radiation (λ = 0.71073 Å) at 293 K by using the ω-scan mode. CrysAlisPro [38] were performed for the data collection, data reduction and empirical absorption correction [39]. The structure was solved by direct methods of SHELXS program [40] within Olex2 [41], and refined by full-matrix least-squares based on F^2 using SHELXL [42]. Anisotropic thermal parameters were assigned to all non-hydrogen atoms. All hydrogen atoms were in calculated positions and refined as riding atoms with fixed isotropic thermal parameters [43].
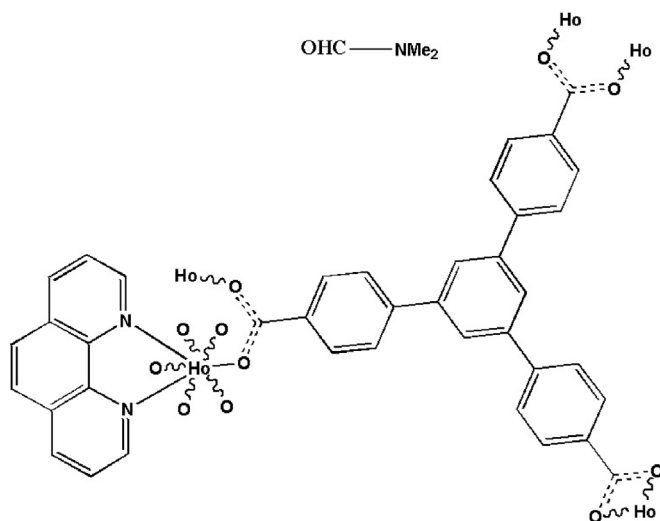
Scheme 1. Ideal conformation of the polymeric compound **1**.

Table 1
Crystal data and structure refinement information for **1**.

CCDC number	1864895
Chemical Formula	$C_{42}H_{30}HoN_3O_7$
Formula weight (g mol^{-1})	853.62
Crystal system	Monoclinic
Space group	P2$_1$/c
Unit cell dimensions	a = 10.7767 (5)Å
	b = 17.6388 (7)Å β = 95.487 (4)°
	c = 21.1028 (12)Å
V/Å^3	3993.0 (3)
Z	4
D$_{calc}$/g cm^{-3}	1.420
μ/mm^{-1}	2.032
F(000)	1704
Temperature (K)	296 (2)
Reflections collected	12864
Independent reflections	7506, [R$_{int}$ = 0.0415]
Goodness–of–fit on F^2	1.029
R indices [$I>2\sigma(I)$]	R_1 = 0.0491, wR_2 = 0.1212

$R_1 = \Sigma||F_0| - |F_c||/\Sigma|F_0|$, $wR_2 = [\Sigma_w (F_0^2 - F_c^2)^2]/\Sigma_w(F_0^2)2]^{1/2}$.

Table 2
Selected bond lengths (Å) and angles (°) for complexes.

Ho1 – N1	2.523(6)	Ho1 – O3^{iii}	2.271(4)
Ho1 – N2	2.560(5)	Ho1 – O4^{i}	2.313(4)
Ho1 – O1	2.261(5)	Ho1 – O5^{iv}	2.423(4)
Ho1 – O2^{ii}	2.326(4)	Ho1 – O6^{iv}	2.394(4)
N1 – Ho1 – N2	63.96(18)	O3^{iii} – Ho1 – N1	82.09(18)
O1 – Ho1 – N1	145.85(18)	O3^{iii} – Ho1 – N2	140.87(16)
O1 – Ho1 – N2	142.19(17)	O3^{iii} – Ho1 – O4^{i}	125.45(15)
O1 – Ho1 – O2^{ii}	126.02(16)	O3^{iii} – Ho1 – O5^{iv}	131.11(14)
O1 – Ho1 – O3^{iii}	76.90(17)	O3^{iii} – Ho1 – O6^{iv}	78.40(14)
O1 – Ho1 – O4^{i}	77.91(16)	O4^{i} – Ho1 – N1	136.08(18)
O1 – Ho1 – O5^{iv}	81.59(17)	O4^{i} – Ho1 – N2	75.76(17)
O1 – Ho1 – O6^{iv}	77.20(17)	O4^{i} – Ho1 – O5^{iv}	91.15(14)
O2^{ii} – Ho1 – N1	72.64(18)	O4^{i} – Ho1 – O6^{iv}	139.60(15)
O2^{ii} – Ho1 – N2	76.11(15)	O5^{iv} – Ho1 – N1	92.65(18)
O2^{ii} – Ho1 – O3^{iii}	75.57(15)	O5^{iv} – Ho1 – N2	72.35(15)
O2^{ii} – Ho1 – O4^{i}	81.72(15)	O5^{iv} – Ho1 – O6^{iv}	54.07(13)
O2^{ii} – Ho1 – O5^{iv}	148.45(16)	O6^{iv} – Ho1 – N1	72.37(19)
O2^{ii} – Ho1 – O6^{iv}	138.62(16)	O6^{iv} – Ho1 – N2	106.97(16)

(Symmetry codes: i= 1-x,-1/2+y,1/2-z; ii= 2-x,1-y,1-z; iii= 1+x,3/2-y,1/2+z; iv= 1-x,1/2+y,1/2-z).

The scattering from the highly disordered lattice quest molecules (DMF) was removed by the SQUEEZE routine and details of the supramolecular π-interactions were obtained PLATON 1.17 program [44]. Crystallographic data together with refinement details and CCDC number for **1** are given in Table 1. Selected bond lengths and angles are reported in Table 2.

3. Result and discussion

3.1. Crystal structure description

The X-ray crystal structure shows that **1** crystallized in monoclinic space group P2$_1$/c. As illustrated in Fig. 1a, the asymmetric unit of 1 consists of one crystallographically unique Ho^{III} ion, one BTB^{3-} and phen ligand and one lattice DMF molecule. Each Ho^{III} ion contains eight co-ordinates to six carboxylic oxygen atoms from BTB^{3-} and two nitrogen atoms from phen ligand, forming a distorted square anti-prismatic co-ordination geometry (Fig. 1b). For all the coordinated oxygen atoms, six of them belong to five carboxylate groups from different BTB^{3-} ligands, while two nitrogen atoms come from the phen ligand. The Ho–O and Ho–N bond distances are in the normal range, varying 2.261(5)–2.423(4) Å and 2.523(6)–2.560(5)Å, respectively [45–47]. The Ho^{III} ion links its symmetry-related atoms to form an {Ho$_2$(COO)$_6$} dinuclear SBU with four bridgings (O1, O2, O3, and O4) and two chelating (O5 and O6) carboxylate groups. Notely, the twisted BTB^{3-} ligands exhibit two different bridging modes: one only acts in ($\kappa^1-\kappa^1$)–μ^1 and the other acts in ($\kappa^1-\kappa^1$)–μ^2, to link the Ho^{III} ions, resulting in the formation of a 3D porous framework with a void volume of 660.3 Å^3 per unit cell (Fig 1), which is 16.5% of total crystal volume (calculated by PLATON) [48–50]. Two crystallographically equivalent Ho^{III} ions are bridged to a dimeric unit as secondary unit buildings (SUBs) by four carboxyl groups in different directions, which also form typical 1D hexagonal channels with BTB^{3-} ligands, these channels are connected in a three-dimensional (3D) framework (Fig. 2). These structures are further stabilized by π···π stacking interactions (Table S1 and Fig. 3).

3.2. Hirshfeld surface analysis

Hirshfeld surface analysis is a valuable implement to evaluated the molecular arrangements and quantify the interactions within the crystal structure [51]. The intermolecular interactions, as well as the surface properties of crystal structure, were obtained by the 3D Hirsrfeld surfaces mapped over d_{norm}, curvedness, shape index and 2D fingerprint plots were successfully generated from CrystalExplorer 17.5 [52] software using the cif data of **1** (Fig. 4) [53–55].

The Hirshfeld surface is mapped using the normalized contact distance dnorm, which is defined using the following equation: $d_{norm} = \{(d_i - r_i^{vdw})/r_i^{vdw}\} + \{(d_e - r_e^{vdw})/r_e^{vdw}\}$, where d_i and d_e are the distance from a point on the surface to the nearest nucleus internal and external the surface, respectively; r_i and r_e are the van der Waals (*vdw*) radii of the

Fig. 1. (a) The Ho^{III} coordination environment of structure **1**, with 50% probability displacement ellipsoids, all hydrogen atoms and noncoordinated DMF molecules are omitted for clarity. Symmetry codes:(i = 1-x,-1/2+y,1/2-z; ii = 2-x,1-y,1-z; iii = 1+x,3/2-y,1/2+z; iv = 1-x,1/2+y,1/2-z; v = −1+x,3/2-y,-1/2+z) and (b) Coordination geometry of Ho^{III} atom in **1** (color online).
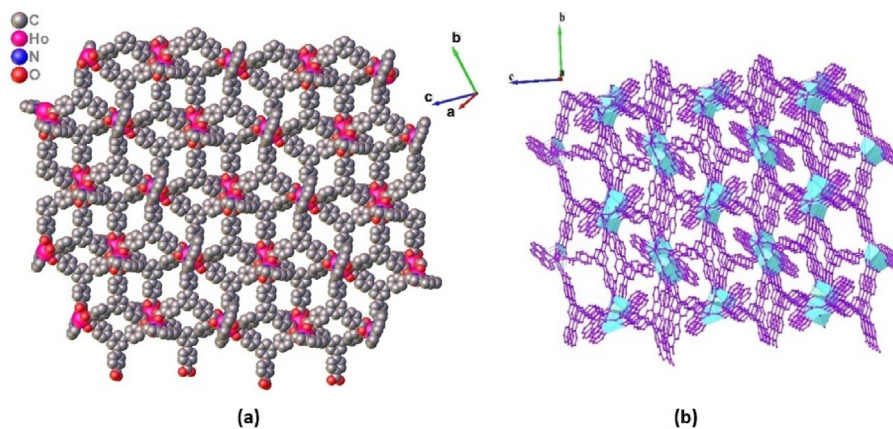
Fig. 2. (a) The illustration of the 2D layer structure (phen molecules and hydrogen atoms are removed from the structure) and (b) A view of the 3D architecture of **1**.
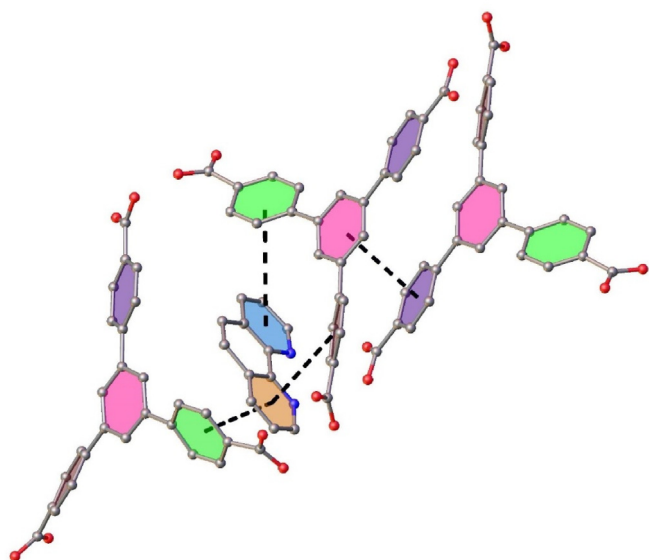

Fig. 3. π⋯π interaction by the phen-btb and btb-btb ligands.

appropriate atom inside outside to the surface respectively. With the help of d_{norm}, it is possible to distinguish between regions participating in intermolecular interactions using the colors of the surface. White, red and blue colors spot have been presented for the visualization of d_{norm}.

The red-colored spots express the most intense contact with atoms near the surface, white is produced due to the intermediate atoms, and the blue spots present weaker contacts with longer distances than the Hirshfeld surface [51]. When mapped with d_{norm}, the surface of **1** produces spherical red depressions that mainly indicate the presence of C–H⋯O type interactions, and other visual depressions attend to H⋯H and C⋯H interactions. The bright red depressions are seen in **1** on the Hirshfeld surfaces, showing that O⋯H/H⋯O interactions are corresponding [56].

The 2D fingerprint plots, which are derivated from 3D Hirshfeld surfaces, give quantitative information on the contribution of crystal structures to the Hirshfeld surfaces and provide a visual summary of the frequency of each de and di combination across the surface of a molecule. Furthermore, two-dimensional (2D) fingerprint plots were mapped over the 3D Hishfeld surface to highlight the nature of the intermolecular interactions and provide a visual summary of all the intermolecular contacts experienced by the molecule quantitatively. Dividing of the fingerprint into specific atom⋯atom contacts in a crystal contributes to a percentage of the different types of intermolecular contact experienced by the molecule [56,57]. As a result, it not only indicates the presence of

intermolecular interactions but also gives information about the relative area of the surface corresponding to each type of interaction.

Shape index and curvature refer to surface properties to determine molecular arrangements in the crystal. Shape index and curvature are metrics that describe local shape in terms of major curvatures. Fig. 4b is a presentation of the shape index, which is a qualitative measure of shape and can be touchy to very little changes in surface shape. Moreover, the shape index of the Hirshfeld surface is a tool to visualize the π⋯π staking by the presence of adjacent red and blue triangles. The red triangles observed on the surface shape from Fig. 4b represent concave regions indicating atoms of the π⋯π stacked molecule above them, whereas the blue triangles represented by convex regions illustrate the aromatic regions of the molecule inside the surface [56].

Similar to the shape index, curvedness plots contain important information about the π⋯π stacked of the molecule (Fig. 4c). In the curvedness plot, large green regions are bordered by dark blue curves. The large flat regions display π⋯π stacking interactions of the molecules while the flat areas of the surface are an indication of interactions between neighboring molecules. Resulting, The π⋯π staking information determined by the shape index and curvature plots is compatible with the crystal structure analyses [56,58,59].

The fingerprint plots highlight the precise atom pair interactions in a crystal. It is a visual representation of all the intermolecular interactions in a crystal structure. Meanwhile, it presents a relative representation of the contributions from all intermolecular interactions. 2D fingerprint plots, which contain C⋯H/H⋯C, H⋯H and O⋯H/H⋯O interactions are illustrated in Fig. 4d-g. The most important interaction of the total Hirshfeld surface area is H⋯H interaction with a contribution of 38.2%. The other major contributions are C⋯H/H⋯C (34.2%) and O⋯H/H⋯O (12.4%) interactions. As can be seen from the above facts, the proportions of H⋯H is relatively stronger than C⋯H/H⋯C and O⋯H/H⋯O interactions [60]. Hirshfeld surface analysis showed that the main structural motifs of the molecular crystal originate from H⋯H, C⋯H and O⋯H interactions, which is in agreement with single-crystal X-ray diffraction analysis.

3.3. Powder X-ray diffraction pattern (PXRD) and thermogravimetric analyses (TGA)

To verify the phase purity of the bulk product, powder X-ray diffraction (PXRD) experiments were carried out on **1**. The X-ray powder diffraction of **1**, and its simulated pattern are closely matched, implying that the bulky material of **1** is formed in high purity and crystallinity (Figs. S1 and SI).

TGA curves can provide an experimental idea for the theoretical prediction of the molecular formula. To research the stability of 1, thermogravimetric analyses (TGA) were performed on a polycrystalline
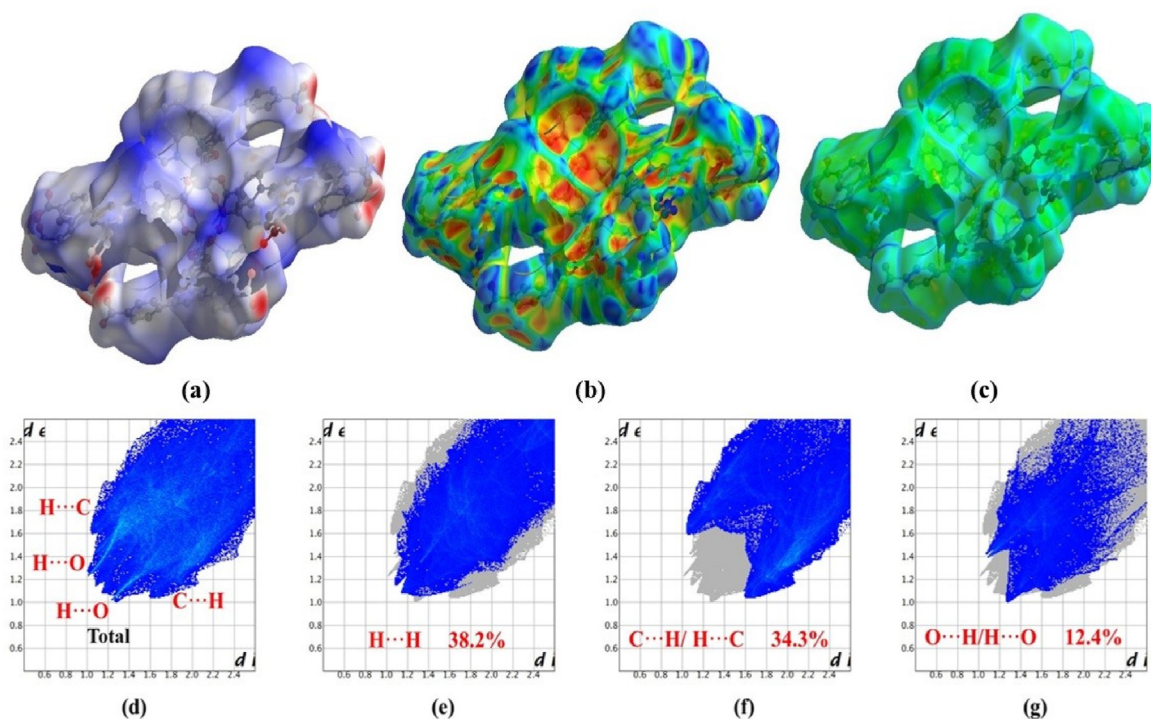
Fig. 4. (a) Hirshfeld surface mapped with d_{norm}, (b) shape index, (c) curvedness, and (d–g) fingerprint plots for **1**.

sample of 1 under a dynamic nitrogen atmosphere. The weight loss of 1 is divided into three-step with increasing temperature (Figs. S2 and SI). In the first step, the weight loss is 29.84% in the range from room temperature to 168 °C which can be attributed to DMF molecule. In the second step, TGA graph displays a weight loss of 17.79% between 226 and 409 °C, equaled the loss of coordinated phen molecules. When the temperature is above 530 °C, the weight loss curve decreases rapidly, which can be attributed to the destructive phenomenon within the structure of the framework [61–64].

3.4. UV–vis and FT-IR spectra

The solid-state absorption spectra of **1** and its free ligands (H₃BTB and phen) were recorded in five well-resolved absorption bands (Fig. 5). The

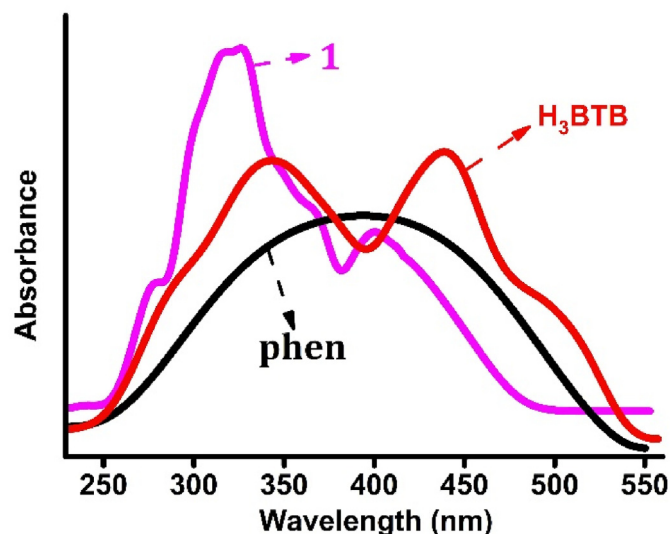**Fig. 5.** The absorption spectra of free H_3BTB and phen ligands and **1**.

absorption bands center at 343 and 439 nm for H_3BTB and 392 nm for phen ligands, respectively. The UV–Vis spectra of **1** show two absorption bands centered at approximately 326 nm and 399 nm. The high energy band observed at ca. 326 nm, which can be assigned to the singlet π-π* transition of the benzene rings and phenol groups from the H_3BTB ligand, while another prominent absorption band at ca. 399 nm, which may be attributed to the n-π* transition of the free ligands [65].

Infrared spectra of 1, H_3BTB and phen have been measured in the range of 4000–600 cm^{-1} (Figs. S3 and SI). The broad bands at around 3408-3298 cm^{-1} that is attributed to the stretching vibrational ν_{O-H} modes, indicating the presence of DMF solvent molecules in the structure [66]. The weak absorption band in the range of 3055–3070 cm^{-1} can be assigned to ν_{C-H}, which is probably attributed to the phen ligand [67]. The strong peak at 1693 cm^{-1} can be attributed to the protonation of carboxyl groups. The absence of this vibration peak in **1** indicates that carboxyl groups of BTB ligand are completely deprotonated and coordinated to Ho^{III} ion [68]. Meanwhile, the peak at 1666 cm^{-1} ($\nu_{C = O}$) and 1581, 1515, 1408 cm^{-1} ($\nu_{C = C}$) can be assigned to the amide bond of the solvent DMF molecules and carbonyl vibrational modes of benzene rings, respectively [50]. Showing strong characteristic peaks absorption near 858 and 783 cm^{-1} in **1**, which is conformity the absorption peaks of BTB and phen ligand, may be attributed to the phenyl and benzene rings of the BTB and phen ligand, respectively [50].

3.5. Morphology

The field emission scanning electron microscope (FESEM) pictures presented information directly about the size and shape of the synthesized compound. The morphology of the surface for the **1** indicates its porous and stratified nature and also was investigated at different magnifications by FESEM pictures (Figs. S4 and SI). FESEM micrographs of the compound have a crack and irregular structures. The pictures showed layered-shaped rough and relatively smooth surface morphology. Their morphology was recorded in different shapes and sizes ranging from 1 μm to 100 μm. The pictures show a smart look with its thin shape or multi-stratified, which indicates crystalline nature. The multi-stratified shape structures result from the accumulation of a great number of

monomers which lead to polymerization [69,70].

3.6. Photo-physical investigations of 1

The luminescent data and spectra of the free ligands (H$_3$BTB and phen) and **1** were collected in the solid-state at room temperature (Figs. S5 and SI and Fig. 6). The free H$_3$BTB ligand shows purple emission at 450 nm and a shoulder attached to a wide band at 565 nm, whereas the free phen ligand shows a broad emission band at $\lambda_{max} = 445$ nm (green light emission) which can be attributed to the electronic transition of the n-π^* or π-π^* (ILCT) [71].

As illustrated in Fig. 6, there is a broad band between 365 and 450 nm in the emission spectrum of **1**, which can be assigned to emission arising from the ligands since it incorporates a suitable conjugated system. Ho^{III} compound shows three characteristic peaks at 521, 575 and 653 nm corresponding to $^5F_3 \rightarrow {}^5I_8, {}^5S_2 + {}^5F_4 \rightarrow {}^5I_8$ and $^5F_5 \rightarrow {}^5I_8$ in the visible region, whereas only one weakly peak at 761 nm originated to $^5S_2 + {}^5F_4 \rightarrow {}^5I_7$ in the NIR region. The characteristic yellow emission of $^5S_2 + {}^5F_4 \rightarrow {}^5I_8$ transition is much stronger than the green emission band of $^5F_3 \rightarrow {}^5I_8$ and the red emission band of $^5F_5 \rightarrow {}^5I_8$, so **1** emits yellowish-orange light. These characteristic peaks are commonly observed in Ho^{III}-compounds. The CIE chromaticity diagram of 1 is illustrated in Fig. 6. The PL emission data of **1** were calculated and marked by a black triangle at (0.480, 0.430). Further analysis of CIE chromaticity coordinates indicates that **1** is an ideal candidate for yellow-orange luminescent materials. Based on this background, **1** may be a promising compound used in the fields of optical materials [72].

Generally, the direct excitation of Ln^{III} ions is very inefficient due to the parity-forbidden nature of the 4f transitions (Laporte) that result in low absorption coefficient and long-living excited. However, indirect excitation of Ln^{III} ions can be performed through an "antenna effect" or "sensitized emission" process that achieves effective sensitizations (Fig. 7) [73]. In the first stage, the free ligands are transited from the ground state (S$_0$) to the excited singlet state (S$_1$), the second stage is the intersystem crossing (ISC) from singlet excited state (S$_1$) to the excited triplet state (T), The next stage is the energy transfer from the T state of the ligand to the excited state of the lanthanide ion. In the last stage, the final energy is transferred to the ground state of the Ln^{III} ion in the form of luminescence released, resulting in the characteristic emission of the Ln^{III} ion [71,74,75]. It is commonly known that the energy transfer in lanthanide-based coordination compounds occurs, as a principle, from the triplet levels of ligand and the efficiency of this process correlates with the energy difference between the triplet levels of ligand and the acceptor levels of the light-emitting Ln^{III} activators [71]. In the present study, to understand the formation of the excited triplet state of H$_3$BTB and phen ligands, as well as the energy transfer pathway of the present complex, we investigated the energy levels of each component. it has been established that the lowest triplet energy level of the H$_3$BTB and
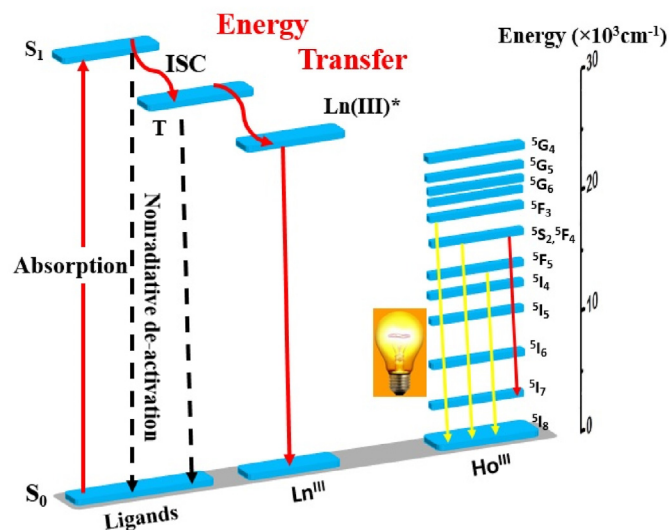

Fig. 7. A schematic representation of the energy transfer mechanism and emissive levels in **1**.

phen ligands are 22.222 and 22.472 cm^{-1} respectively, and the emitting level ($^5F_3$) of Ho^{III} lies at 19.194 cm^{-1}. The energy gap between **1** and H$_3$BTB and phen are approximately calculated at 3028 and 3278 cm^{-1}, respectively. We emphasize that these energy differences are the optimum values for efficient energy transfer from the excited triplet levels of ligands to Ho^{III} emitting level [71,74–76].

4. Conclusion

In summary, a new Ho^{III}-Organic Framework, {[Ho(BTB)(phen)].(DMF)}$_n$, (H$_3$BTB = 1,3,5-Tris(4-carboxyphenyl) benzene, phen = 1,10-Phenanthroline monohydrate and DMF = N,N–Dimethylformamide), with H$_3$BTB and phen as ancillary ligands were synthesized with the solvothermal route. Prepared complex were successfully characterized structurally, morphologically and spectroscopically. 3D porous Ho^{III} organic framework has been constructed based on BTB^{3-} and phen ligand. Notably, Ho^{III} ions are bridged to a dimeric unit by four carboxyl groups in different directions, which also form typical 1D hexagonal channels with BTB^{3-} ligands, resulting in the formation of a 3D porous framework with a void volume of 660.3 Å^3 per unit cell. This result not only provides an aesthetic structural diversity but also allows the creation of new porous materials with various metal structural units to produce networks with large pores and high connectivity modes. According to the 3D Hirshfeld surface and 2D fingerprint plots, H···H intermolecular interactions are the dominant interactions in the Ho^{III}
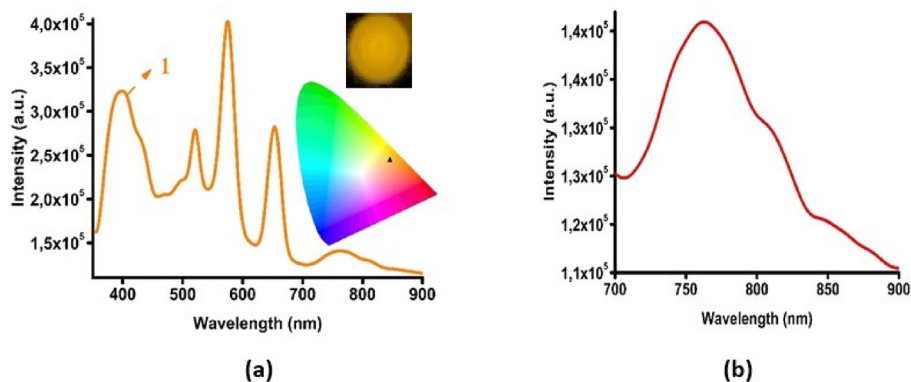

Fig. 6. (a)The corresponding emission spectrum in the vis-NIR region (355–900 nm) (inset: Upper-right photo is a photoluminescent image of **1** while excited at 349 nm and bottom-right photo is its CIE chromaticity diagram image) and (b) the emission spectrum of **1** in the NIR region (700–900 nm).

with a contribution of 38.2%. Besides, the π···π stacking information determined by the shape index and curvedness plots coincides with the crystal structure analysis. The solid-state photoluminescence measurements show that Ho[III] derivatives exhibit very strong and characteristic luminescence emissions in the visible region after excitation by ultraviolet radiation, thus forming promising materials for luminescent probes. Thus, we speculate that lanthanide-containing hybrid materials could be used as intermediate materials in LEDs and/or photoluminescence sensors. Besides, it is thought that Ho[III] complex may be a potential candidate that can be used for active luminescence material purposes in terms of use.

CRediT authorship contribution statement

Mustafa Burak Coban: Visualization, Methodology, Conceptualization, Investigation, Software, Writing – original draft, Writing – review & editing.

Declaration of competing interest

The authors declare that they have no known competing financial interests or personal relationships that could have appeared to influence the work reported in this paper.

Data availability

Data will be made available on request.

Acknowledgments

Appendix A. Supplementary data

Supplementary data to this article can be found online at https://doi.org/10.1016/j.jssc.2022.123651.

References

[1] B. Sherino, S. Mohamad, N.S. Abdul Manan, H. Tareen, B.M. Yamin, S.N. Abdul Halim, Structural, electrochemical, and adsorption studies of Ni and Zn benzylimidazole coordination polymers with terephthalate linkers, Transit. Met. Chem. 43 (2018) 53–64.

[2] A. Hernández-Morales, J.M. Rivera, A. López-Monteon, S. Lagunes-Castro, S. Castillo-Blum, K. Cureño-Hernández, A. Flores-Parra, O. Villaseñor-Granados, R. Colorado-Peralta, Complexes containing benzimidazolyl-phenol ligands and Ln(III) ions: synthesis, spectroscopic studies and preliminary cytotoxicity evaluation, J. Inorg. Biochem. 201 (2019), 110842.

[3] E. Otgonbaatar, M.-C. Chung, K. Umakoshi, C.-H. Kwak, Preparation and luminescent property of the self-assembled nanoscale network systems combined tetracyanoplatinate(II) and copper(II)-Polyaza complexes, J. Nanosci. Nanotechnol. 15 (2015) 1389–1395.

[4] M. Kariem, M. Kumar, M. Yawer, H.N. Sheikh, Solvothermal synthesis and structure of coordination polymers of Nd(III) and Dy(III) with rigid isophthalic acid derivatives and flexible adipic acid, J. Mol. Struct. 1150 (2017) 438–446.

[5] M.S. Salman, M.M.N. Hasan, K.T. Kubra, M.M.N. Hasan, Optical detection and recovery of Yb(III) from waste sample using novel sensor ensemble nanomaterials, Microchem. J. 162 (2021), 105868.

[6] M.B. Coban, Magnetic and photophysical properties of new Tb[III] –based two-dimensional hydrogen-bonded polymer, J. Mol. Struct. 1177 (2019) 331–337.

[7] D. Zhao, Y.-L. Xue, Y.-C. Fan, R.-J. Zhang, S.-R. Zhang, A new series of rare-earth borate-phosphate family CsNa2Ln2(BO3)(PO4)2 (Ln = Ho, Er, Tm, Yb): tunnel structure, upconversion luminescence and optical thermometry properties, J. Alloys Compd. 866 (2021), 158801.

[8] S. Yoopensuk, P. Tongying, K. Hansongnern, C. Pakawatchai, S. Saithong, Y. Tantirungrotechai, N. Leesakul, Photoactive azoimine dyes: 4-(2-Pyridylazo)-N,N-diethylaniline and 4-(2-pyridylazo)-N,N-dimethylaniline: computational and experimental investigation, Spectrochim, Acta Part A Mol. Biomol. Spectrosc. 86 (2012) 538–546.

[9] C. Pagis, M. Ferbinteanu, G. Rothenberg, S. Tanase, Lanthanide-based metal organic frameworks: synthetic strategies and catalytic applications, ACS Catal. 6 (2016) 6063–6072.

[10] S. Bibi, S. Mohamad, N.S.A. Manan, J. Ahmad, M.A. Kamboh, S.M. Khor, B.M. Yamin, S.N. Abdul Halim, Synthesis, characterization, photoluminescence, and electrochemical studies of novel mononuclear Cu(II) and Zn(II) complexes with the 1-benzylimidazolium ligand, J. Mol. Struct. 1141 (2017) 31–38.

[11] V. Placide, A.T. Bui, A. Grichine, A. Duperray, D. Pitrat, C. Andraud, O. Maury, Two-photon multiplexing bio-imaging using a combination of Eu- and Tb-bioprobes, Dalton Trans. 44 (2015) 4918–4924.

[12] Q.-F. Lin, L.-L. Ding, Z.-H. Xu, Q. Wang, N.-F. Li, Y. Xu, L.-L. Liang, Three 3D Lanthanide coordination polymers: synthesis, luminescence and magnetic properties, J. Mol. Struct. 1234 (2021), 130167.

[13] Y. Zhang, J.-M. Zheng, Three Ln(III)-2,3,5-trichlorobenzoate coordination polymers (Ln = Tb, Ho and Er): syntheses, structures and magnetic properties, Inorg. Chem. Commun. 59 (2015) 21–24.

[14] S. Alghool, M.S. Zoromba, H.F.A. El-Halim, Lanthanide amino acid Schiff base complexes: synthesis, spectroscopic characterization, physical properties and in vitro antimicrobial studies, J. Rare Earths 31 (2013) 715–721.

[15] S. Kongchoo, A. Kantacha, S. Saithong, S. Wongnawa, Synthesis, crystal structure, and spectroscopic properties of Cu(II) complex with 14-membered hexaazamacrocyclic ligands, J. Chem. Crystallogr. 46 (2016) 222–229.

[16] R. Abazari, E. Yazdani, M. Nadafan, A.M. Kirillov, J. Gao, A.M.Z. Slawin, C.L. Carpenter-Warren, Third-order nonlinear optical behavior of an amide-tricarboxylate zinc(II) metal–organic framework with two-fold 3D+3D interpenetration, Inorg. Chem. 60 (2021) 9700–9708.

[17] H. Xu, F. Zhong, F. Chen, T.-X. Luan, P. Li, S. Xu, J. Gao, A Zr-MOF nanoflower sensor and its mixed-matrix membrane for the highly sensitive detection of nitroaromatics, J. Mater. Chem. C 10 (2022) 7469–7475.

[18] V. Orsi Gordo, Y. Tuncer Arslanli, A. Canimoglu, M. Ayvacikli, Y. Galvão Gobato, M. Henini, N. Can, Visible to infrared low temperature luminescence of Er3+, Nd3+ and Sm3+ in CaSnO3 phosphors, Appl. Radiat. Isot. 99 (2015) 69–76.

[19] S. Son, H. Lee, C. Kwak, J. Lee, H. Ahn, M. Chung, A study of phosphorescent light emitting using cyclometalated Pt(II) complexes, J. Nanosci. Nanotechnol. 15 (2015) 5338–5341.

[20] K.S. Smirnova, E.A. Ivanova, T.S. Sukhikh, I.P. Pozdnyakov, V.V. Dotsenko, E.V. Lider, Luminescent properties of Ln(III) complexes with 2-[(phenylamino) methylene]-5,5-dimethyl-cyclohexane-1,3-dione as an antenna, Inorg. Chim. Acta. 525 (2021), 120490.

[21] Y. Liang, D. Mao, X. Guo, J. Yu, G. Wu, Z. Ma, Solvothermal preparation of CuO-ZnO-ZrO2 catalysts for methanol synthesis via CO2 hydrogenation, J. Taiwan Inst. Chem. Eng. 121 (2021) 81–91.

[22] L. Huang, Z. Luo, Y.-N. Zhou, Q. Zhang, H. Zhu, S. Zhu, Solvothermal synthesis of covalent triazine framework and its application in photodegradation of organic dyes, Mater. Today Chem. 20 (2021), 100475.

[23] X. Wang, M. Chen, M. Du, A clear insight into the distinguishing CO2 capture by two isostructural Dy III –carboxylate coordination frameworks, Inorg. Chem. 55 (2016) 6352–6354.

[24] W. Meng, Z. Lin, R. Zhong, L. Kong, R. Zou, A new (3,8)-connected pillared-layer lanthanide–organic framework with interconnected channel and mesoporous cage, Inorg. Chem. Commun. 53 (2015) 50–54.

[25] J.-H. Qin, B. Ma, X.-F. Liu, H.-L. Lu, X.-Y. Dong, S.-Q. Zang, H. Hou, Ionic liquid directed syntheses of water-stable Eu– and Tb–organic-frameworks for aqueous-phase detection of nitroaromatic explosives, Dalton Trans. 44 (2015) 14594–14603.

[26] H. Chen, G.-L. Zhuang, L. Fan, X. Zhang, L.-N. Gao, D. Sun, A highly robust heterometallic Tb III/Ni II –organic framework for C 2 hydrocarbon separation and capture, Chem. Commun. 56 (2020) 2047–2050.

[27] K. Sheng, W.-D. Si, R. Wang, W.-Z. Wang, J. Dou, Z.-Y. Gao, L.-K. Wang, C.-H. Tung, D. Sun, Keggin-type tridecanuclear europium-oxo nanocluster protected by silsesquioxanes, Chem. Mater. 34 (2022) 4186–4194.

[28] M.B. Coban, Hydrothermal synthesis, crystal structure, luminescent and magnetic properties of a new mononuclear Gd III coordination complex, J. Mol. Struct. 1162 (2018) 109–116.

[29] Y. Acar, M.B. Coban, E. Gungor, H. Kara, Two new NIR luminescencent Er(III) coordination polymers with potential application optical amplification devices, J. Cluster Sci. 31 (2020) 117–124.

[30] C. Wang, Y. Xing, Z. Li, J. Li, X. Zeng, M. Ge, S. Niu, A new series of lanthanide coordination polymers with 2,2′-bipyridine and glutaric acid: synthesis, crystal structures and properties of [Ln(bipy)(glut)(NO3)], J. Mol. Struct. 931 (2009) 76–81.

[31] S.A. Cotton, O.E. Noy, F. Liesener, P.R. Raithby, Unequivocal characterisation of a [Ln(terpy)(NO3)3·(H2O)] complex, Inorg. Chim. Acta. 344 (2003) 37–42.

[32] J.-G. Kang, T.-J. Kim, H.-J. Kang, Y. Park, M.-K. Nah, Structural and luminescence properties of [Ln(ODA)(phen)·4H2O]+ complexes (Ln=Sm and Dy, ODA=oxydiacetate, phen=1,10-phenanthroline), J. Lumin. 128 (2008) 1867–1872.

[33] P.R.S. Santos, D.K.S. Pereira, I.F. Costa, I.F. Silva, H.F. Brito, W.M. Faustino, A.N. Carneiro Neto, R.T. Moura, M.H. Araujo, R. Diniz, O.L. Malta, E.E.S. Teotonio, Experimental and theoretical investigations of the [Ln(β-dik)(NO3)2(phen)2]·H2O luminescent complexes, J. Lumin. 226 (2020), 117455.

[34] H. Xu, B. Zhai, C.-S. Cao, B. Zhao, A bifunctional europium–organic framework with chemical fixation of CO 2 and luminescent detection of Al 3+, Inorg. Chem. 55 (2016) 9671–9676.

[35] T.N. Nguyen, G. Capano, A. Gładysiak, F.M. Ebrahim, S.V. Eliseeva, A. Chidambaram, B. Valizadeh, S. Petoud, B. Smit, K.C. Stylianou, Lanthanide-based near-infrared emitting metal–organic frameworks with tunable excitation wavelengths and high quantum yields, Chem. Commun. 54 (2018) 6816–6819.

[36] P. Meng-Qi, Y. Run-Qi, M. Yaseen, C. Kun-Tong, H. Feng, Z. Hao-Chen, N. Yuan-Qing, W. Hao, Crystal structure, Fe3+ luminescence sensing and color tuning of 2D lanthanide-metal-organic frameworks constructed from tricarboxylic acid ligand, Jiegou Huaxue 41 (2022) 2202023–2202033.

[37] X.-M. Chen, M.-L. Tong, Solvothermal in situ metal/ligand reactions: a new bridge between coordination chemistry and organic synthetic chemistry, Acc. Chem. Res. 40 (2007) 162–170.

[38] CrysAlisPro, Rigaku Oxford Diffraction, Version 1.171.39.6a.

[39] R.C. Clark, J.S. Reid, The analytical calculation of absorption in multifaceted crystals, Acta Crystallogr. Sect. A Found. Crystallogr. 51 (1995) 887–897.

[40] G.M. Sheldrick, A short history of SHELX, Acta Crystallogr. Sect. A Found. Crystallogr. 64 (2008) 112–122.

[41] O.V. Dolomanov, L.J. Bourhis, R.J. Gildea, J.A.K. Howard, H. Puschmann, OLEX2 : a complete structure solution, refinement and analysis program, J. Appl. Crystallogr. 42 (2009) 339–341.

[42] G.M. Sheldrick, Crystal structure refinement with SHELXL, Acta Crystallogr. Sect. C Struct. Chem. 71 (2015) 3–8.

[43] Y. Yahsi, X-ray characterization and magnetic properties of dioxygen-bridged Cu II and Mn III Schiff base complexes, Acta Crystallogr. Sect. C Struct. Chem. 72 (2016) 585–592.

[44] A.L. Spek, Structure validation in chemical crystallography, Acta Crystallogr. Sect. D Biol. Crystallogr. 65 (2009) 148–155.

[45] M. Hu, H. Zhao, E.C. Sañudo, M. Chen, Four lanthanide–carboxylate coordination polymers with mixed 2,3-naphthalenedicarboxylate and phen ligands: syntheses, structures, luminescent and magnetic properties, Polyhedron 101 (2015) 270–275.

[46] U.P. Singh, N. Goel, G. Singh, P. Srivastava, Syntheses, structural and thermal studies of Eu(III) and Gd(III) complexes with 2,6-dinitrophenol and 1,10-phenanthroline/2,2′-bipyridine ligands, Inorg. Chim. Acta. 387 (2012) 294–307.

[47] M.-M. Zhu, J. Cui, Y.-L. Zeng, N. Ren, J.-J. Zhang, Two novel Sm(III) complexes with different aromatic carboxylic acid ligands: synthesis, crystal structures, luminescence and thermal properties, Polyhedron 158 (2019) 485–493.

[48] H. Zhang, X. Shan, Z. Ma, L. Zhou, M. Zhang, P. Lin, S. Hu, E. Ma, R. Li, S. Du, A highly luminescent chameleon: fine-tuned emission trajectory and controllable energy transfer, J. Mater. Chem. C 2 (2014) 1367.

[49] C.-M. Liu, D.-Q. Zhang, Y.-S. Zhao, X. Hao, D.-B. Zhu, Two-step warming solvothermal syntheses, luminescence and slow magnetic relaxation of isostructural dense LnMOFs based on nanoscale 3-connected linkers, Inorg. Chem. Front. 3 (2016) 1076–1081.

[50] Z. Lin, R. Zou, W. Xia, L. Chen, X. Wang, F. Liao, Y. Wang, J. Lin, A.K. Burrell, Ultrasensitive sorption behavior of isostructural lanthanide–organic frameworks induced by lanthanide contraction, J. Mater. Chem. 22 (2012) 21076.

[51] O. Boukhemis, L. Bendjeddou, C. Platas-Iglesias, D. Esteban-Gómez, M. Carcelli, H. Merazig, Hydrothermal synthesis of six new lanthanides coordination polymers based on 1-H-benzimidazole-5-carboxylic acid: structure, Hirshfeld analysis, thermal and spectroscopic properties, Inorg. Chim. Acta. 510 (2020) 119740.

[52] M.J. Turner, J.J. McKinnon, S.K. Wolff, D.J. Grimwood, P.R. Spackman, D. Jayatilaka, CrystalExplorer17 5 (2017).

[53] M.A. Spackman, D. Jayatilaka, Hirshfeld surface analysis, CrystEngComm 11 (2009) 19–32.

[54] J.J. McKinnon, A.S. Mitchell, M.A. Spackman, Hirshfeld surfaces: a new tool for visualising and exploring molecular crystals, Chem. Eur J. 4 (1998) 2136–2141.

[55] J.J. McKinnon, M.A. Spackman, A.S. Mitchell, Novel tools for visualizing and exploring intermolecular interactions in molecular crystals, Acta Crystallogr. Sect. B Struct. Sci. 60 (2004) 627–668.

[56] L.L. Cai, Y.T. Hu, Y. Li, K. Wang, X.Q. Zhang, G. Muller, X.M. Li, G.X. Wang, Solid-state luminescence properties, Hirshfeld surface analysis and DFT calculations of mononuclear lanthanide complexes (Ln = EuIII, GdIII, TbIII, DyIII) containing 4′-phenyl-2,2′:6′,2″-terpyridine, Inorg. Chim. Acta. 489 (2019) 85–92.

[57] L.-L. Cai, S.-M. Zhang, Y. Li, K. Wang, X.-M. Li, G. Muller, F.-P. Liang, Y.-T. Hu, G.-X. Wang, Lanthanide nitrato complexes bridged by the bis-tridentate ligand 2,3,5,6-tetra(2-pyridyl)pyrazine: syntheses, crystal structures, Hirshfeld surface analyses, luminescence properties, DFT calculations, and magnetic behavior, J. Lumin. 232 (2021) 117835.

[58] H.H. Sallam, Y.H.E. Mohammed, F.H. Al-Ostoot, M.A. Sridhar, S.A. Khanum, Synthesis, structure analysis, DFT calculations, Hirshfeld surface studies, and energy frameworks of 6-Chloro-3-[(4-chloro-3-methylphenoxy)methyl][1,2,4]triazolo[4,3-b]pyridazine, J. Mol. Struct. 1237 (2021), 130282.

[59] S. Kumaresan, R.N. Asha, J.M. Libiyal, V.A. Selvam, N. Bhuvanesh, B.R.D. Nayagam, Growth, structural, Hirshfeld surface analysis, DFT validation on the crystal structure of 1, 10-Phenanthrolin-1-ium-5,6-dione perchlorate monohydrate, Chem. Data Collect. 33 (2021), 100706.

[60] Q. Zhao, X.-X. An, L.-Z. Liu, W.-K. Dong, Syntheses, luminescences and Hirshfeld surfaces analyses of structurally characterized homo-trinuclear ZnII and hetero-pentanuclear ZnII-LnIII bis(salamo)-like complexes, Inorg. Chim. Acta. 490 (2019) 6–15.

[61] H. Wang, S. Jiang, L. Xiang, Y. Yan, G. Xiang, Y. Li, X. Luo, L. Li, X. Tang, X. Zhou, Synthesis and characterization of Tb3+/Eu3+ complexes based on 2,4,6-tris(4-carboxyphenyl)-1,3,5-triazine ligand for ratiometric luminescence temperature sensing, Spectrochim. Acta Part A Mol. Biomol. Spectrosc. 244 (2021) 118781.

[62] S. Ullah, M.A. Bustam, M.A. Assiri, A.G. Al-Sehemi, G. Gonfa, A. Mukhtar, F.A. Abdul Kareem, M. Ayoub, S. Saqib, N.B. Mellon, Synthesis and characterization of mesoporous MOF UMCM-1 for CO2/CH4 adsorption; an experimental, isotherm modeling and thermodynamic study, Microporous Mesoporous Mater. 294 (2020), 109844.

[63] R. Ilmi, K. Iftikhar, Structure elucidation by sparkle/RM1, effect of lanthanide contraction and photophysical properties of lanthanide(III) trifluoroacetylacetonate complexes with 1,10-phenanthroline, J. Photochem. Photobiol. Chem. 325 (2016) 68–82.

[64] L.-C. Wang, J. Sun, Z.-T. Huang, Q.-Y. Zheng, Stepwise tuning of the substituent groups from mother BTB ligands to two hexaphenylbenzene based ligands for construction of diverse coordination polymers, CrystEngComm 15 (2013) 8511.

[65] E. Gungor, 3-D polymeric structure formed by hydrogen bonds of copper (II) complex, Mol. Cryst. Liq. Cryst. 642 (2017) 21–28.

[66] E. Gungor, A new stepped tetranuclear copper(II) complex: synthesis, crystal structure and photoluminescence properties, Acta Crystallogr. Sect. C Struct. Chem. 73 (2017) 393–398.

[67] M. Daqqa, A.A. AlObaid, N. Al-Zaqri, F.F. Awwadi, A. Zarrouk, A. Alsalme, R. Alasmari, A. Karami, I. Warad, Ultrasonic synthesis, XRD/HSA-interactions, DFT, time-dependence spectrophotometric stability and thermal analysis of the water-bridge {[Cu(phen)2Br]Br·H2O} complex, J. King Saud Univ. Sci. 33 (2021), 101464.

[68] J. Ran, X. Zhao, X. Hu, Y. Chen, Z. Tian, 3D Tb(III) and Eu(III) coordination polymers with mixed dicarboxylate ligands: synthesis, structure and luminescence properties, Polyhedron 194 (2021), 114910.

[69] B. Ay, E. Yildiz, İ. Kani, Two novel isostructural and heteroleptic Nd(III) and Dy(III)-organic frameworks constructed by 2,5-pyridinedicarboxylic acid and in situ generated 2-pyridinecarboxylic acid: hydrothermal synthesis, characterization, photoluminescence properties and hetero, Polyhedron 130 (2017) 165–175.

[70] B. Ay, E. Yildiz, İ. Kani, Semiconducting lanthanide polymers of pyridine-2,6-dicarboxylate: hydrothermal synthesis, structural characterization, electrical conductivity and luminescence properties, Polyhedron 142 (2018) 1–8.

[71] G. Zhang, X. Xia, L. Xia, F. Sun, J. Dong, R. Li, H. Wu, A series of new hetero-decanucleus sandwich Cd–Ln clusters constructed from open-chain ether Schiff base and niacin ligands: synthesis, structure, luminescence and antioxidant activity, Inorg. Chim. Acta. 522 (2021) 120371.

[72] J.-Y. Zhao, N. Ren, J.-J. Zhang, Supramolecular of lanthanide-2,6-dimethylbenzoic acid-2,2′:6′,2″-terpyridine materials: crystal structures, luminescent property, and thermochemical behaviour, Polyhedron 194 (2021), 114892.

[73] A. Cruz-Navarro, D. Hernández-Romero, A. Flores-Parra, J.M. Rivera, S.E. Castillo-Blum, R. Colorado-Peralta, Structural diversity and luminescent properties of coordination complexes obtained from trivalent lanthanide ions with the ligands: tris((1H-benzo[d]imidazole-2-yl)methyl)amine and 2,6-bis(1H-benzo[d]imidazole-2-yl)pyridine, Coord. Chem. Rev. 427 (2021), 213587.

[74] M. Kaczmarek, Lanthanide-sensitized luminescence and chemiluminescence in the systems containing most often used medicines; a review, J. Lumin. 222 (2020), 117174.

[75] Y. Qu, C. Wang, Y. Wu, H. Wu, X. Han, J. Xu, X. Xia, Construction of d-f heteronuclear complexes with open-chain ether Schiff base ligand: regulation effects of Zn(II) and Cd(II) on structures and luminescence properties, J. Lumin. 226 (2020), 117437.

[76] N. Hasan, K. Iftikhar, Luminescence from a highly asymmetric nine-coordinate tricapped trigonal prismatic Sm(III) complex, J. Lumin. 223 (2020), 117135.